Wavelet-Based Monitor for Grid Impedance Estimation of Three-Phase Networks

Alves, Denis Keuton; Ribeiro, Ricardo Lucio De Araujo; Costa, Flavio Bezerra; Rocha, Thiago De Oliveira Alves; Guerrero, Josep M.

Published in:
IEEE Transactions on Industrial Electronics

DOI (link to publication from Publisher):
10.1109/TIE.2020.2972460

Publication date:
2021

Document Version
Accepted author manuscript, peer reviewed version

Wavelet-Based Monitor for Grid Impedance Estimation of Three-Phase Networks

Denis K. Alves, Ricardo L. A. Ribeiro, *Member*, *IEEE*,
Flavio B. Costa, *Member*, *IEEE*, Thiago O. A. Rocha, and Josep M. Guerrero, *Fellow*, *IEEE*

***Abstract*—This paper proposes a wavelet-based monitor (WBM) for grid-impedance estimation, which combines a wavelet-based transient detection scheme (WB-TDS) and a wavelet-based grid impedance estimator (WB-GIE). The WB-TDS employs the analysis of the wavelet coefficients energy for detecting grid impedance changing, whereas the WB-GIE estimates the grid-impedance by using the real-time stationary discrete wavelet packet transform (RT-SDWPT) associated with signal injection scheme. During a grid impedance changing, the WB-TDS triggers the WB-GIE for injecting an interharmonic into the power grid to estimate its current impedance. This method mitigates the THD generated by the continuous signal injection employed in the existing techniques. The WB-GIE identifies the phase grid impedance resistance and reactance accurately in balanced or unbalanced conditions. Due to its inherent characteristics, WBM is suitable to be inserted into the adaptive power flow control of distributed generation systems. Experimental results obtained from a grid-connected photovoltaic generation laboratory setup validated the proposed method and demonstrated its effectiveness.**

***Index Terms*—Grid impedance estimation, steady-state active method, wavelet transform.**

I. Introduction

THE insertion of renewable energy sources as distributed generations (DG) modified the composition of the power system following the modern concept of the microgrid. In this model, the DG sources interconnect the grid via power converters as active front-end (AFE) that regulate the power flow in any direction [1], [2], which demanded efforts for achieving robustness and reliability. Therefore, to maintain these DGs as secure supplies with suitable power quality has become more challenging. Besides, AFEs must operate in both grid-connected and islanded modes, requiring modifications in the power flow control strategy. In general, the AFE control systems employ droop methods for regulating the active and reactive power injection by regulating the frequency and amplitude of the output voltage [3]. However, conventional droop approaches depend on the grid parameters to decouple the control of active and reactive power flows [4]. Therefore, the knowledge of grid impedance can contribute to suitable control operation decisions, providing inputs for load flow studies, DGs dispatchability, protection, or detection of islanding conditions [5]. Thus, the implementation of an embedded strategy to estimate grid impedance has excellent utility in the power flow control and operation of the actual power system [6].

Different methods could be employed to estimate grid impedance whose implementation can follow passive or active approaches [6]. Passive approaches use the information of noncharacteristic voltage and current harmonics, already present in the system, to estimate the grid impedance [7]. Therefore, these techniques employ the existing structures of control and acquisition for implementing grid impedance estimation algorithms. Regarding this approach, the controlled excitation of the frequency characteristic of an LCL-based inverter demonstrated to be an alternative for estimating the impedance of grid-connected inverters [8]. A recursive least-square (RLS) technique for analyzing voltages and currents of the DG interface was another method for obtaining the grid equivalent impedance [9]. Another possibility is to estimate the grid impedance by processing voltage, and current phasors at the point of common coupling (PCC) derived from a frequency-locked loop based on a second-order generalized integrator (SOGI-FLL) [4]. Extended Kalman Filter (EKF) can analyze the PCC voltages and currents to estimate the power network impedance [10]. Also, it is possible to use the discretized grid-tied model in a rotating reference frame to evaluate the grid inductance and resistance [11]. However, passive approaches present a drawback related to the inherent low signal-to-noise ratio (SNR), which can compromise the accuracy of the grid impedance estimation [11].

Active methods that employ a signal injection to estimate the grid impedance overcome drawbacks of passive techniques [11]. Their implementation can follow transient or steady-state techniques [6]. Transient methods employ noncharacteristic signal injections as voltage disturbance, or current spike to estimate the grid impedance over a wide frequency range via a postprocessing procedure [5], [12]–[14]. The drawback of using the voltage disturbance as signal injection refers to its dependence on existing harmonic distortion due to the presence of moderate power electronic loads. Instead, the injection

Manuscript received April 1, 2019; revised September 27, 2019 and December 27, 2019; accepted January 22, 2020. This work was supported by the Brazilian National Council for Scientific and Technological Development (CNPq).

D. K. Alves, R. L. A. Ribeiro, F. B. Costa, and T. O. A. Rocha are with the Federal University of Rio Grande do Norte (UFRN), Natal, Brazil (e-mail: alvesk3@hotmail.com, rlucio@ct.ufrn.br, flaviocosta@ect.ufrn.br, and thiago.rocha@ct.ufrn.br).

J. M. Guerrero is with the Department of Energy Technology, Aalborg University, 9220 Aalborg East, Denmark (Tel: +45 2037 8262; Fax: +45 9815 1411; e-mail: joz@et.aau.dk). J. M. Guerrero was funded by a Villum Investigator grant (no. 25920) from The Villum Fonden.

of a current spike showed to be more efficient to minimize these disturbances [12]. This signal analysis generates much more data than needed and can overload the real-time control algorithm of power interfaces. An alternative is to use the steady-state approach based on a periodic interharmonic signal injection and analyze the system response [6].

Both transient and steady-state active methods usually use the discrete Fourier transform (DFT) that is dependent on existing harmonic distortions and susceptible to power electronic loads. These estimation approaches can be ineffective during transient events and lead to wrong interpretations due to spectral leakage and picket-fence effects. The use of continuous wavelet transformer (CWT), with a complex mother wavelet, instead of DFT demonstrated to be an alternative to overcome these limitations [15]. However, the CWT is not usually embedded in real-time applications due to its complexity.

The discrete wavelet transform (DWT) versions, such as the stationary discrete wavelet packet transform (SDWPT), with real mother wavelet, have been used successfully as an alternative to the CWT in several practical applications. However, DWT versions with real mother wavelet present mathematical limitations for estimating phase angle [16]. Based on this statement, the DWT has been claimed to be unsuitable for impedance estimation [15], and no method based on it was available in the literature. Nevertheless, [17] demonstrates recently that a cross-analysis of both voltage and current system response overcomes the lack of phase information and makes the SDWPT-based impedance estimation viable for real-time applications. The method proposed in [17], based on a steady-state active approach, injects an interharmonic component continuously into the power system to estimate the grid impedance, which can result in power quality deviations in the PCC. Moreover, important issues such as time duration and magnitude of the signal injection, as well as the best choice of the mother wavelet, were not assessed in [17]. Besides, [17] presents no mechanism to identify when the grid impedance needs to be estimated.

Active steady-state methods inject controlled voltage or current signals (interharmonic, step signals, etc.) into the reference controlled system, provoking disturbances, and power quality problems (harmonic distortions) [18]. To overcome this drawback, a hybrid strategy composed of the integration of transient approach and a Luenberger observer modified the estimation algorithm to only provide the signal injection when grid impedance changes occur [19]. This strategy improves the THD when compared with the alternative proposed by [17] by constraining the signal injection to those time intervals related to the grid changes, but still has the DFT restrictions related before. Also, the insertion of the estimation method into the control strategy generates grid-impedance estimates on the stationary reference frame, which could introduce errors in unbalanced conditions due to the lack of homopolar component information [20].

In the same direction, this paper proposes a wavelet-based monitor (WBM) for grid-impedance estimation, which combines a power system transient detection (WB-TDS) and a grid impedance estimation (WB-GIE) approaches both using wavelet-based techniques. The WB-TDS employs the analysis of the wavelet coefficient energy to detect transit events. According to [21], the first level wavelet coefficient energy can be used for the high-speed detection of voltage sag, faults, nonstationary disturbances, or switching maneuver due to a fast increase of energy in the disturbance inception time. For instance, when the network is subject to any disturbance, such as the grid impedance change, the WB-TDS detects it and triggers the WB-GIE. Therefore, the WB-GIE injects a non-characteristic signal (interharmonic component) into the PCC for a fast and accurate estimation of the power grid impedance using the SDWPT method. The WBM restricts the signal injection to a small-time interval, and low-level interharmonic required for an accurate grid impedance estimation without inducing power quality problems into the grid.

Furthermore, the WB-GIE estimates the grid impedance resistance and reactance of each PCC phase and correlates it with the previous results for showing the dynamic evolution. The WB-GIE employs a compact mother wavelet for avoiding a long-duration signal injection. Due to their inherent characteristics, the WBM demonstrates to be suitable for integrating power flow adaptive control strategies applied for DG systems. Experimental results obtained from a photovoltaic (PV) distributed generation laboratory setup validated the proposed method and demonstrated its effectiveness and feasibility.

II. System Modeling and Control

Fig. 1 shows the laboratory setup of the DG system implemented by a grid-tied PV system based on dual-stage conversion topology. It comprises a three-phase PV system with a rated power of 8 kWp interconnected to a power grid implemented by a 15 kVA three-phase indoor substation. The dc-dc boost converter regulates the dc-link voltage and implements the MPPT by changing its duty-cycle. An LCL filter interconnects the PV voltage source inverter (VSI) to the PCC. Controlled switches $K5$, $K6$ and $K7$ interconnect three-phase linear or nonlinear loads to the PCC for emulating different operational scenarios. The controlled switches $K1$ - $K4$, together with the external components r_{test} and l_{test}, allow for the modification of the nominal grid impedance (r_g and l_g). This structure permits the emulation of weak-grid with different R/X rates or unbalanced conditions.

The value of the short-circuit ratio (SCR) defines the grid strength. Considering the system in Fig. 1, where the value of short-circuit power is S_{SC} = 50.3 kVA and the nominal power of the distributed generation is S_n = 8 kWp, the SCR is computed as follows [22]:

$$SCR = \frac{S_{SC}}{S_n} = \frac{50300}{8000} \approx 6.3, \qquad (1)$$

in which SCR < 10 addressing to a weak-grid condition according to [23]. The PV-based DG system employs the most commonly multiloop control strategy applied for grid-tied LCL converter, also presented in Fig. 1. The inner control loop regulates output phase currents, and the outer control loop sets the dc-link voltage. The controller $R_v(s)$ regulates the DC-link voltage based on the system energy balance, by determining the amplitude of the PV system output

This article has been accepted for publication in a future issue of this journal, but has not been fully edited. Content may change prior to final publication. Citation information: DOI 10.1109/TIE.2020.2972460, IEEE Transactions on Industrial Electronics

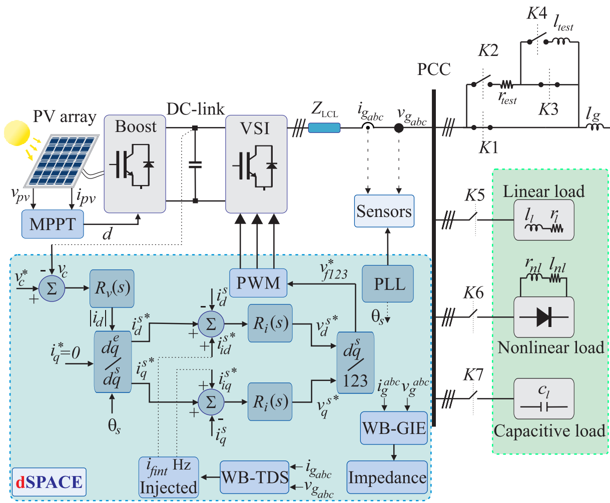

Fig. 1. Block diagram of the 8 kWp PV three-phase laboratory setup.

vector current $|i_d|$ imposed by the controllers $R_i(s)$. They are implemented on the stationary reference frame with their bandwidths adjusted for allowing the required interharmonic injection. Both blocks WB-TDS and WB-GIE implement the proposed grid-impedance estimation scheme (WBM). The integration of WB-GIE to the DG control system results in modified reference currents composed by interharmonic injection added to standard track currents (i.e, $i_{dq}^{s*'} = i_{dq}^{s*} + i_{idq}^{s*}$), in which the superscript s represents the stationary reference frame. The WB-GIE injects the interharmonic in the stationary reference frame, but both WB-TDS and WB-GIE use three-phase voltages and currents, which permit the grid changing detection and the grid impedance estimation in each PCC phase. Therefore, the WBM provides accurate estimation results, even though the power system operates under unbalanced conditions.

III. Basis of The Proposed WBM Estimator

The proposed WBM employs the real-time SDWPT (RT-SDWPT) to implement the network transient detection and grid impedance estimation strategies.

A. The Real-Time Wavelet Packet Coefficients

The RT-SDWPT decomposition packet coefficients at level j are computed as follows [24]:

$$s_j^{2z}(k) = \frac{1}{\sqrt{2}} \sum_{l=0}^{L-1} h_\varphi(l) s_{j-1}^z(k+l-L+1), \tag{2}$$

$$s_j^{2z+1}(k) = \frac{1}{\sqrt{2}} \sum_{l=0}^{L-1} h_\psi(l) s_{j-1}^z(k+l-L+1), \tag{3}$$

where $0 \leq z \leq 2^{j-1}-1$ is the node number; s_j^z is the wavelet packet coefficients associated to the node z at scale j; $s_0^0 = x$ represents the original signal; L is the length of the wavelet filter; k is the current sampling associated to the time k/f_s, where f_s is the sampling rate; h_φ and h_ψ are low- and high-pass finite impulse response (FIR) quadrature mirror filters.

Based on [25], the spectral energy ($\mathcal{E}$) of a signal x in terms of the SDWPT, at any scale j, is given by:

$$\mathcal{E}(k) = \sum_{n=k-\Delta k+1}^{k} |x(n)|^2 = \mathcal{E}_{j,x}^0(k) + \sum_{z=1}^{2^j-1} \mathcal{E}_{j,x}^z(k), \tag{4}$$

where

$$\mathcal{E}_{j,x}^0(k) = \frac{1}{2\Delta k} \sum_{n=k-\Delta k+1}^{k} \sum_{l=0}^{L-1} \left[s_{j,x}^0(k-l)\right]^2, \tag{5}$$

$$\mathcal{E}_{j,x}^z(k) = \frac{1}{2\Delta k} \sum_{n=k-\Delta k+1}^{k} \sum_{z=1}^{2^j-1} \sum_{l=0}^{L-1} \left[s_{j,x}^z(k-l)\right]^2, \tag{6}$$

where $k \geq \Delta k$-1, $\mathcal{E}_{j,x}^0$ is the energy of wavelet packet coefficients of the lowest frequency band at node zero and level j, whereas $\mathcal{E}_{j,x}^z(k)$ is the energy of wavelet packet coefficients at node $z \neq 0$; Δk is the number of samples per cycle of the power system frequency (f = 50 or 60 Hz).

B. Estimation of Power Components with RT-SDWPT

The RT-SDWPT can estimate the main power components according to the IEEE Standard 1459-2010 [26], useful for accomplishing the accurate grid impedance estimation.

1) The RMS Values: The discrete time-domain signal $x(k)$ can be described in terms of the RF-SDWPT coefficients as follows ($s_{j,x}^z$) [24]:

$$x(k) = \frac{1}{\sqrt{2}} \sum_{l=0}^{L-1} h_\varphi(l) s_{j,x}^0(k-l) + \frac{1}{\sqrt{2}} \sum_{z=1}^{2^j-1} \sum_{l=0}^{L-1} h^z(l) s_{j,x}^z(k-l). \tag{7}$$

The filter h is defined as follows:

$$h^{2z} = h_\varphi \quad \text{and} \quad h^{2z+1} = h_\psi. \tag{8}$$

The signal $x(k)$ can also be termed in function of the wavelet packet coefficient energy as follows [24]:

$$[x(k)]^2 = \frac{1}{2}\left[\sum_{l=0}^{L-1} (\mathcal{E}_{j,x}^0(k-l))^2 + \sum_{z=1}^{2^j-1} \sum_{l=0}^{L-1} (\mathcal{E}_{j,x}^z(k-l))^2\right]. \tag{9}$$

Therefore, the wavelet-based RMS value is given by [24]:

$$X_w(k) = \sqrt{\frac{1}{2\Delta k} \sum_{n=k-\Delta k+1}^{k} \left[\sum_{z=0}^{2^j-1} (X_j^z(n))^2\right]}, \tag{10}$$

where $X_w = V_w$ for voltage or $X_w = I_w$ for current, and

$$X_j^z(n) = \sqrt{\sum_{l=0}^{L-1} (\mathcal{E}_{j,x}^z(n-l))^2}. \tag{11}$$

is the wavelet-based RMS value at node z.

From (10) in (11), the wavelet-based RMS voltage is given by:

$$V_w(k) = \sqrt{\frac{1}{2\Delta k} \sum_{n=k-\Delta k+1}^{k} \left[\sum_{z=0}^{2^j-1} \sum_{l=0}^{L-1} (\mathcal{E}_{j,v}^z(n-l))^2\right]}. \tag{12}$$

Similarly, the wavelet-based RMS current is given:

$$I_w(k) = \sqrt{\frac{1}{2\Delta k} \sum_{n=k-\Delta k+1}^{k} \left[\sum_{z=0}^{2^j-1} \sum_{l=0}^{L-1} (\mathcal{E}_j^z{}_{,i}\,(n-l))^2 \right]}. \quad (13)$$

2) Power Components: The active power can also be described in terms of the RT-SDWPT coefficients as follows:

$$P_w(k) = \frac{1}{\Delta k} \sum_{n=k-\Delta k+1}^{k} v(k)i(k), \quad (14)$$

where $v(k)i(k)$ in wavelet terms is given by [24]:

$$v(k)i(k) = \frac{1}{2} \sum_{l=0}^{L-1} s_j^0{}_{,v}\,(k-l) s_j^0{}_{,i}\,(k-l) + \frac{1}{2} \sum_{z=1}^{2^j-1} \sum_{l=0}^{L-1} s_j^z{}_{,v}\,(k-l) s_j^z{}_{,i}\,(k-l). \quad (15)$$

Therefore, substituting (15) in (14) yields [24]:

$$P_w(k) = \frac{1}{2\Delta k} \sum_{n=k-\Delta k+1}^{k} \left[\sum_{l=0}^{L-1} \mathcal{E}_j^0{}_{,v}\,(n-l) \mathcal{E}_j^0{}_{,i}\,(n-l) + \sum_{z=1}^{2^j-1} \sum_{l=0}^{L-1} \mathcal{E}_j^z{}_{,v}\,(n-l) \mathcal{E}_j^z{}_{,i}\,(n-l) \right], \quad (16)$$

where $P_w(k)$ represents the total active power of the frequency band associated to the node z and level j. (16) is in accordance with the Parseval's theorem.

From (10), the wavelet-based apparent power is given by

$$S_w(k) = V_w(k) I_w(k). \quad (17)$$

Based on the classical power theory, the wavelet-based power factor is given by:

$$PF_w(k) = \frac{P_w(k)}{S_w(k)}. \quad (18)$$

IV. The Proposed Grid Changing Detection - WB-TDS

The implementation of the proposed WB-TDS employs the analysis of the wavelet coefficient energy for detecting transient network events based on [21]. According to this method, the wavelet coefficients of power system voltages and currents, at the first decomposition level, present a Gaussian probability distribution function with zero mean ($\mu_w \approx 0$) and a standard deviation (σ_w), termed as $N(0,\, \sigma_w^2)$, with harmonics disregarded in this related wavelet sub-band. In this fashion, the wavelet coefficient energy in the steady-state is only affected by high-frequency noises and can be employed to detect disturbances through established thresholds, which follows the chi-square probability distribution [27]. Therefore, the occurrence of any grid disturbance (e.g., faults, voltage sag, nonstationary disturbances, switching maneuver, etc.) produce an increase of the wavelet coefficient energy providing a high-speed detection of the grid-impedance changing, which follows a simple criterion:

$$\mathcal{E}_{1,\{v,i\}}^1(k-1) < E \quad \text{and} \quad \mathcal{E}_{1,\{v,i\}}^1(k) > E, \quad (19)$$

where $\mathcal{E}_{1,\{v,i\}}^1$ represents the energy of wavelet coefficients of the node one in the first level, at the frequency band [480, 960] Hz (s_1^1) and E is an energy threshold stochastically defined in [27] as two times of the steady-state average energy level and, hence, when (19) is verified, the proposed WB-TDS triggers the WB-GIE for injecting a synthesized interharmonic into the power grid for estimating its impedance.

V. The Proposed Grid Impedance Estimator - WB-GIE

The proposed WB-GIE method estimates the grid impedance by injecting a temporary interharmonic (i_{fint}) to the PV control system reference currents. The use of this noncharacteristic signal injection relies on the fact that under standard operational such frequency component does not exist in the system. Moreover, the chosen interharmonic must have a frequency higher than the fundamental, with low magnitude and short duration to avoid interference in the power grid performance. The suggested frequency is addressed in this Section, whereas its magnitude and duration will be discussed in Section VI.

A. Sampling Rate and the Decomposition Level

According to the Nyquist criterion, a discrete signal with the sampling rate of f_s has frequency band components limited from 0 to f_s/2. From the multiresolution analysis, it is possible to decompose an input signal in various frequency sub-bands with different resolution levels. The SDWPT employs the multiresolution analysis, obtained through the inner product of an input signal with a quadrature mirror filter pair (low- and high-pass filters). The extraction of the synthetic interharmonic component depends on both the sampling rate and wavelet decomposition level. Firstly, the fundamental and the harmonics must be located on the cutoff frequencies of the wavelet filters, which means that f_s must be multiple integers of $8f$. Besides that, the synthetic interharmonic must be centered in one of the wavelet sub-bands to ensure superior performance in its component extraction.

For instance, employing a sampling frequency of $f_s = 1920$ Hz with a fundamental frequency of f = 60 Hz (32 samples per cycle), it is necessary four decomposition levels (j = 4). Therefore, the frequency spectrum is divided into sixteen bands with a regular 60-Hz interval, with the fundamental and harmonic components located on cutoff frequencies of these bands. For improving the grid impedance estimation and avoiding the side-effects due to the fundamental and low-order harmonics of the power grid, it is essential to choose the interharmonic frequency far from them. One possible solution is to select the interharmonic frequency of f_{int} = 630 Hz. Fig. 2 presents the decomposition tree to extract the interharmonic component of this example, with the synthesized interharmonic centralized at the band [600 - 660] Hz in the fourth decomposition level.

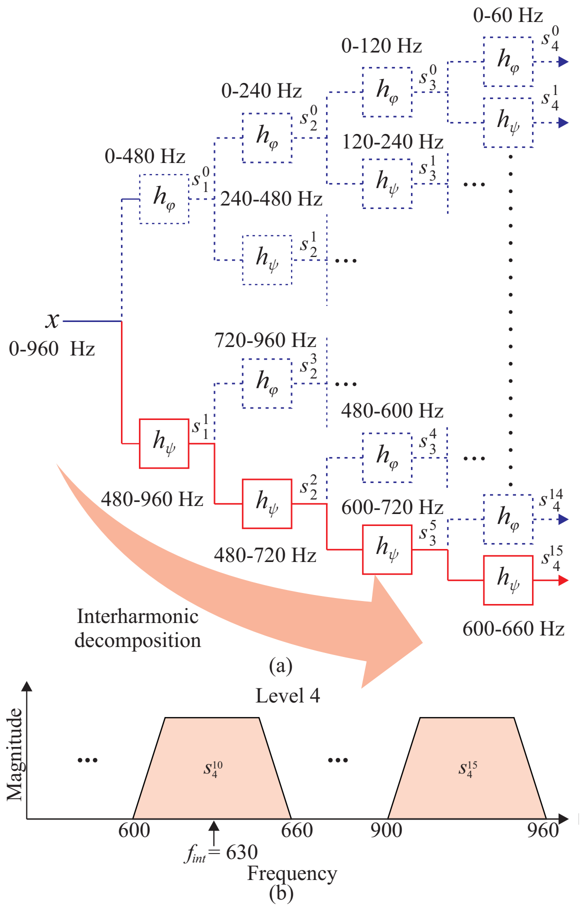

Fig. 2. Wavelet-packet decomposition for a sampling frequency of 1920 Hz: (a) four-level decomposition tree; (b) ideal frequency response.

B. Estimating the Grid Impedance of the Power Grid

Based on (10), the RMS interharmonic voltage and current are computed as follows:

$$V_{f_{int}}(k) = \sqrt{\frac{1}{2\Delta k}\sum_{n=k-\Delta k+1}^{k}\left[\sum_{l=0}^{L-1}(\mathcal{E}_{j,v}^{f_{int}}(n-l))^2\right]}, \quad (20)$$

$$I_{f_{int}}(k) = \sqrt{\frac{1}{2\Delta k}\sum_{n=k-\Delta k+1}^{k}\left[\sum_{l=0}^{L-1}(\mathcal{E}_{j,i}^{f_{int}}(n-l))^2\right]}, \quad (21)$$

where $\mathcal{E}_{j,v}^{f_{int}}$ and $\mathcal{E}_{j,i}^{f_{int}}$ are wavelet coefficient energies of the voltage and current, respectively, at node z and scale j which include the interharmonic frequency f_{int} in the band center.

It is well-known that the SDWPT with a real mother wavelet cannot provide the phase information of a single signal, such as a voltage or a current directly. However, the phase angle difference between the current and voltage can be properly computed using power concepts as follows [17]:

$$P_{f_{int}}(k) = \frac{1}{2\Delta k}\sum_{n=k-\Delta k+1}^{k}\left[\sum_{l=0}^{L-1}\mathcal{E}_{j,v}^{f_{int}}(n-l)\mathcal{E}_{j,i}^{f_{int}}(n-l)\right], \quad (22)$$

$$PF_{f_{int}}(k) = \frac{P_{f_{int}}(k)}{S_{f_{int}}(k)} = \frac{P_{f_{int}}(k)}{V_{f_{int}}(k)I_{f_{int}}(k)}, \quad (23)$$

$$\theta_{f_{int}}(k) = \cos^{-1}(PF_{f_{int}}(k)) = \cos^{-1}\left[\frac{P_{f_{int}}(k)}{V_{f_{int}}(k)I_{f_{int}}(k)}\right], \quad (24)$$

where $\theta_{f_{int}}$ is the phase difference between the voltage and current, which is associated with the phase angle impedance of the interharmonic.

The interharmonic impedance ($\widehat{Z}_{f_{int}}(k)$) can be properly computed by using the RT-SDWPT approach as follows [17]:

$$\widehat{Z}_{f_{int}}(k) = \frac{V_{f_{int}}(k)}{I_{f_{int}}(k)}\angle\,\theta_{f_{int}}, \quad (25)$$

where the real part of $\widehat{Z}_{f_{int}}(k)$ refers to the resistance of the grid impedance as follows [17]:

$$R_g^w(k) = \mathrm{Re}\{\widehat{Z}_{f_{int}}(k)\} = Z_{f_{int}}(k)\cos(\theta_{f_{int}}(k)), \quad (26)$$

whereas the reactance related to the interharmonic frequency corresponds to the imaginary part of $\widehat{Z}_{fint}(k)$ given by [17]:

$$X_{f_{int}}^w(k) = \mathrm{Im}\{\widehat{Z}_{f_{int}}(k)\} = Z_{f_{int}}(k)\sin(\theta_{f_{int}}(k)), \quad (27)$$

The grid reactance is given by [17]:

$$X_g^w(k) = X_{f_{int}}^w(k)\frac{\omega_1}{\omega_{f_{int}}}, \quad (28)$$

where ω_{int} and ω_1 are frequencies of the interharmonic and fundamental components, respectively.

VI. Performance Assessment

The proposed WBM method employs the experimental platform depicted in Fig. 1 for validating its performance. A dSPACE platform executes both the control and estimation algorithms. Take into account the selected interharmonic has the frequency of $f_{int} = 630$ Hz, the current regulators employed in the PV-based DG were redesigned for providing a closed-loop bandwidth of $\omega_{Ri} \cong 1320\pi\ rad/s$ to guarantee the effective signal injection. The commissioning experimental tests fulfill the WBM desired performance by setting up the mother wavelet length, the interharmonic magnitude, and the signal injection duration.

Several measurements realized at different times along the day results in an expected grid impedance of $Z_g \approx 0.53+j0.15$ (i.e., $R_g \approx 0.53\ \Omega$ and $X_g \approx 0.15\ \Omega$), with a deviation of $\pm 10\%$. Based on these measurements, this work adopted the grid impedance of $Z_g \approx 0.53 + j0.155$ as a reference value employed to validate the estimation methods that will be tested in the following experiments.

A. Definition of the Mother Wavelet Length

The WB-GIE implementation can use long or compact mother wavelets. For evaluating those effects, the WB-GIE performs the grid impedance estimation with several mother wavelets. Table I summarizes the used mother wavelets and the average values of the estimated grid impedance.

In [6], a DFT-based method for estimating grid impedance considers the injection of an interharmonic with a frequency of 90 Hz, which is close to the fundamental component. This method injects the interharmonic signal continuously. For the sake of comparison with the proposed method, this

This article has been accepted for publication in a future issue of this journal, but has not been fully edited. Content may change prior to final publication. Citation information: DOI 10.1109/TIE.2020.2972460, IEEE Transactions on Industrial Electronics

existing method was adapted to estimate the grid impedance considering the interharmonic frequency of 630 Hz instead of 90 Hz. Table I demonstrates the performance of both estimation approaches.

According to Table I, both long and compact mother wavelets provided similar performance and agreed with the expected values. However, long mother wavelets present the highest computational burden and highest time delay, leading to drawbacks on real-time applications because it requires long-duration interharmonic injection. Therefore, the mother wavelet db(4) is the most suitable. The WB-GIE provided similar performance to the DFT-based method. However, its use in the proposed WBM produces superior results because the injection of the interharmonic occurs only when the WB-TDS detects a grid impedance changing.

TABLE I
GRID IMPEDANCE ESTIMATION OBTAINED WITH RT-SDWPT-BASED METHOD WITH DIFFERENT MOTHER WAVELETS .

Description	Mother wavelet				DFT
	db(4)	db(6)	db(14)	db(30)	
Resistance [Ω]	0.53	0.53	0.53	0.53	0.53
Reactance [Ω]	0.15	0.15	0.15	0.15	0.15
Impedance [Ω]	0.55	0.55	0.55	0.55	0.55

B. Magnitude of the Interharmonic

The accuracy of the grid impedance estimation depends on both the magnitude and the repetition rate of the interharmonic injection. Small amplitudes can deteriorate the impedance estimation due to the SNR, whereas high amplitudes can increase the total harmonic distortion of output currents ($\mathrm{THD_i}$). To achieve a suitable magnitude level, the WB-GIE performed the grid impedance estimation with different interharmonic amplitudes and compared them with the DFT-based method described before. Table II summarizes the average values of the impedance estimation obtained with both methods by using different interharmonic amplitudes, and associated with: apparent power, shortcircuit power, system SNR, and the $\mathrm{THD_i}$ deviation.

The experimental results presented satisfactory and accurate impedance estimation with low- and high-magnitude of the injected interharmonic while demonstrated that their amplitudes did not influence the estimation. However, the use of interharmonic with higher amplitude could result in significant THDi deviations (see Table II). Therefore, the criterion for the selection of the interharmonic amplitude should consider the THD impact on the grid. Furthermore, the small deviations of impedance values verified in Table II for the same interharmonic magnitude are due to the variation of the penetration level that occurred during the tests.

C. Duration of the Interharmonic Injection

Another critical issue for the implementation of the WB-GIE is the signal injection duration. Continuous signal injection increases the THD, causing possible power quality problems. An alternative is to provide the signal injection for a short period, triggered by the proposed WB-TDS. The advantage of this method is the mitigation of the harmonic distortion. This paper adopted a duration time of the signal injection of 100 ms (six cycles of the fundamental) to avoid undesired power quality issues. Therefore, WB-GIE estimates the grid impedance during this time interval after the detection of a possible grid impedance variation. At the end of this interval, the WB-GIE provides the average value of the grid impedance estimation on the last two cycles.

D. Experimental Results

The performance evaluation and effectiveness of the proposed WBM grid impedance estimator employ four experimental tests in the following operational scenarios: (i) balanced grid impedance variation, (ii) interconnection of three-phase nonlinear load, (iii) unbalanced grid impedance, and (iv) interconnection of a three-phase capacitive load. In all experimental tests, controlled switches $K1-K4$ provide the interconnection of external components $r_{test} = 0.5\ \Omega$ and $l_{test} = 0.5$ mH (inserted simultaneously or individually) in series with the power grid, modifying its nameplate impedance. Table III presents the setup parameters obtained from the commissioning tests. The WB-GIE employs four decomposition levels with a synthetic interharmonic. The decomposition process is only accomplished on the bottom levels of the tree, as highlighted in Fig. 2.

1) Balanced Grid Impedance Variation: Fig. 3 depicts the phase current waveform on the PCC and the grid impedance estimation obtained through the proposed WBM. At the beginning of the experiment, the startup algorithm triggers the WB-GIE for injecting the interharmonic and estimates the power grid impedance, which resulted in $R_g^w \approx 0.53\ \Omega$, $X_g^w \approx 0.15\ \Omega$ and $Z_g^w \approx 0.57\ \Omega$, as presented in Figs. 3(b)-(d), which follows the expected values of $Z_g \approx 0.53 + j0.15$ Ω, with ±10% of deviation. At $t \approx$ 1.65 s, switches $K1-K4$ interconnect the external components (r_{test} and l_{test}) in series with the grid, causing a transient in the currents, as shown in Fig. 3(a) and (e). The WB-TDS detected the grid impedance variation through a fast increase of the first-level wavelet coefficient energy, as shown in Fig. 3(e), which triggers the WB-GIE (flag signal in Fig. 3(a)) for injecting an interharmonic and providing the grid impedance estimation $R_g^w \approx 1.20\ \Omega$, $X_g^w \approx 0.37\ \Omega$ and $Z_g^w \approx 1.22\ \Omega$ (Figs. 3(b)-(d)), which corresponds to the expected impedance (i.e., $Z_g \approx 0.53{+}j0.15$ Ω in series with $Z_{test} \approx 0.5 + j0.188\ \Omega$). In this test, the estimated grid reactance presented a deviation of less than 10% of the predicted value, inside the impedance range imposed by the PV penetration variation. At $t \approx$ 2.90 s, the switches $K1-K4$ removed the external components, provoking another disturbance, also detected by WB-TDS that triggered the WB-GIE to re-estimate the grid impedance. The interharmonic employed in this test was 2.12 A.

2) Interconnection of Nonlinear Load: The interconnection of nonlinear loads at the PCC can result in incorrect impedance estimations [13]. To evaluate the effectiveness of the proposed method, under these operational conditions, switches $K5$ and

This article has been accepted for publication in a future issue of this journal, but has not been fully edited. Content may change prior to final publication. Citation information: DOI 10.1109/TIE.2020.2972460, IEEE Transactions on Industrial Electronics

TABLE II
GRID IMPEDANCE ESTIMATION WITH DIFFERENT MAGNITUDE OF THE INTERHARMONIC.

Magnitude of the interharmonic	Apparent power [kVA]	S_{SC} [kVA]	SNR	THD$_i$ (χ)	THD$_i$ (✓)	Grid impedance [Ω] R_w	R_{DFT}	X_w	X_{DFT}
0.71A	5.40	50.3	35.52 dB	3.34%	7.40%	0.58	0.60	0.17	0.16
0.71A	6.20	50.3	35.42 dB	3.37%	6.77%	0.58	0.61	0.17	0.15
1.41A	5.83	50.3	35.50 dB	3.33%	12.20%	0.57	0.58	0.16	0.16
1.41A	6.49	50.3	35.37 dB	3.35%	11.35%	0.59	0.59	0.16	0.15
2.12A	5.94	50.3	35.47 dB	3.42%	16.62%	0.54	0.54	0.15	0.15
2.12A	6.23	50.3	35.47 dB	3.34%	16.00%	0.57	0.57	0.15	0.15

χ: Before interharmonic injection.
✓: During interharmonic injection.

TABLE III
PARAMETERS USED FOR THE GRID IMPEDANCE ESTIMATION

Frequency of the Interharmonic	630 Hz
Magnitude of the interharmonic	0.71-2.12 A
Duration of the signal injection	6 cycles of the fundamental frequency
Window size	Δk = 64 samples
Sampling rate	1920 Hz

$K6$ (Fig.1) interconnected linear and nonlinear loads simultaneously. Fig. 4 depicts the grid impedance estimation of this experiment. Initially, the estimated impedance has the same values as the test before. At $t \approx 0.4$ s, controlled switches $K5$ and $K6$ interconnect the linear and nonlinear loads at PCC provoking a transient. The WB-TDS detects this disturbance and triggers the WB-GIE for injecting the interharmonic for estimating the grid impedance. The obtained results demonstrated a slight variation in the grid impedance estimates, as expected.

At $t \approx 1.0$ ss, the switches $K1-K4$ interconnected r_{test} in series to the PCC, producing a disturbance, which was detected by the WB-TDS that triggered the WB-GIE for performing the grid impedance estimation. The estimated results are $R_g^w \approx 1.10$ Ω, $X_g^w \approx 0.16$ Ω and $Z_g^w \approx 1.10$ Ω, demonstrating that only the equivalent resistance modified, as expected (the initial value is $R_g^w \approx 0.53$). At $t \approx 1.8$ s, controlled switches $K1-K4$ removed r_{test}, and WBM re-estimated the PCC grid impedance, resulting in the same values of the beginning of the experiment. This test demonstrated that the proposed method produced accurate results even under the presence of nonlinear loads interconnected to the PCC.

3) Unbalanced Grid Impedance: The knowledge of the grid-impedance under the unbalanced condition is essential for determining the stability limits of power system operation, especially in low voltage network systems. Fig. 5 shows the experimental results of the grid impedance estimation when the power grid is unbalanced. Initially, the estimated grid impedance has the same values of the tests realized before. At $t \approx 1.0$ s, the controlled switches $K1-K4$ interconnect r_{test} and l_{test} in series with the phases A and B of the PCC to emulate a grid impedance asymmetry. The WB-TDS detected the transient event in both PCC phases and triggered the WB-GIE for estimating the grid impedances of both PCC phases, which resulted in $R_{ga}^w \approx 1.25$ Ω, $X_{ga}^w \approx 0.37$ Ω, and $Z_{ga}^w \approx 1.35$ Ω for phase A, and $R_{gb}^w \approx 1.10$ Ω, $X_{gb}^w \approx 0.36$ Ω, and $Z_{ga}^w \approx 1.17$ Ω for phase B. The impedance values of phase C remained the same. At $t \approx 2.4$ s, switches $K1-K4$ removed the external components, and the estimated impedance provided by WBM corresponded to the startup values. Power grid employed in the experimental setup has a slight asymmetry, accentuated by the interconnection of the external components. This experiment showed that WBM is also effective in unbalanced PCCs.

4) Interconnection of the Capacitive Load: Fig. 6 depicts the grid impedance estimation of the PCC interconnected to a capacitive bank (provided by the switch $K7$ in Fig. 1). At the beginning of the experiment, the estimated grid impedance has the same values as the last tests. At $t \approx 0.4$ s, switches $K1-K4$ inserted external components in series with the PCC, causing a transient event, detected by the WB-TDS, which triggered the WB-GIE for estimating the grid impedance. The results obtained are $R_g^w \approx 1.10$ Ω, $X_g^w \approx 0.38$ Ω and $Z_g^w \approx 1.20$ Ω. At $t \approx 1.4$ s, the switch $K7$ interconnected the three-phase capacitive load (c_l = 150 μF or X_c= -17.38 Ω) in parallel to the PCC, provoking a disturbance. Therefore, the WBM re-estimated the grid impedance as $R_g^w \approx 1.00$ Ω, $X_g^w \approx 0.34$ Ω, and $Z_g^w \approx 1.12$ Ω, which corresponds to the expected impedance of the equivalent circuit. Theoretically, the parallel association of the impedance $Z \approx 1.10 + j0.38$ Ω, the capacitive load of $X_c = -j17.38$, results in an equivalent impedance of $Z \approx 1.14 + j0.32$ Ω. The WBM estimated the equivalent grid resistance and reactance with acceptable error margins of 12.28% and 6.25%, respectively. This test also demonstrated the effectiveness of the WBM for grid impedance estimation in the PCC interconnected to capacitor banks.

Table IV summaries experimental results related to all operational scenarios.

E. Computational Burden

The computational burden (i.e., the number of multiplications, additions, and other floating-point operations) must be less than the sampling time ($1/f_s$). The proposed grid

This article has been accepted for publication in a future issue of this journal, but has not been fully edited. Content may change prior to final publication. Citation information: DOI 10.1109/TIE.2020.2972460, IEEE Transactions on Industrial Electronics

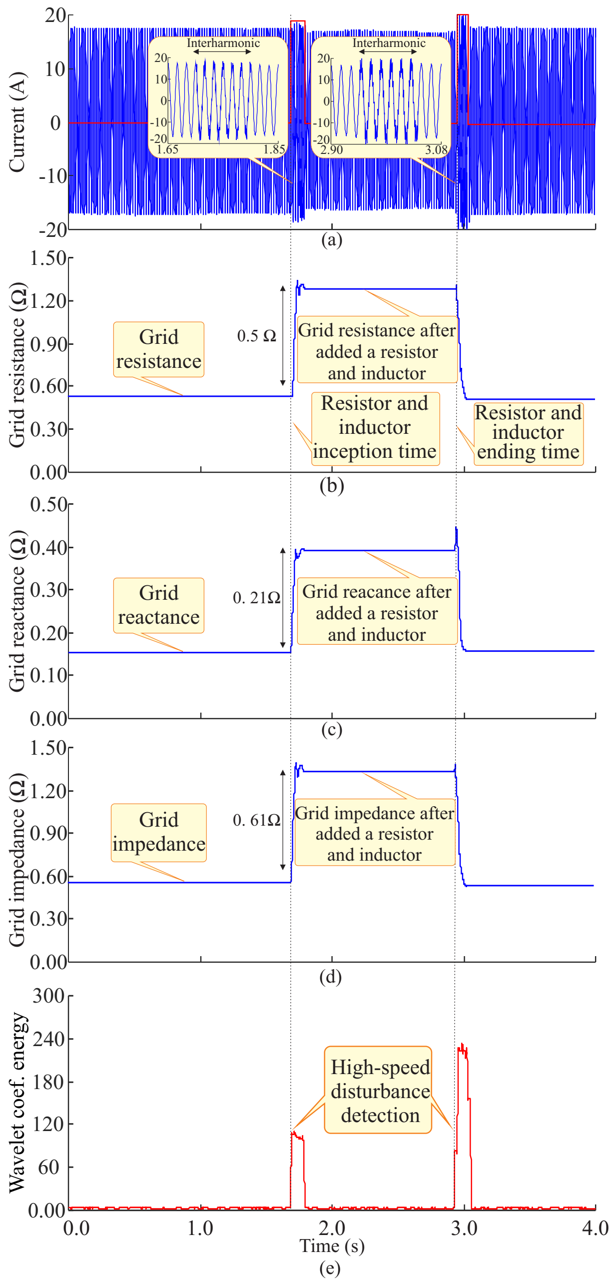

Fig. 3. Real-time grid impedance estimation: (a) time-domain current waveform (blue line) and transient detection flag (red line); (b) grid resistance; (c) grid reactance; (d) grid impedance and; (e) wavelet coefficient energy.

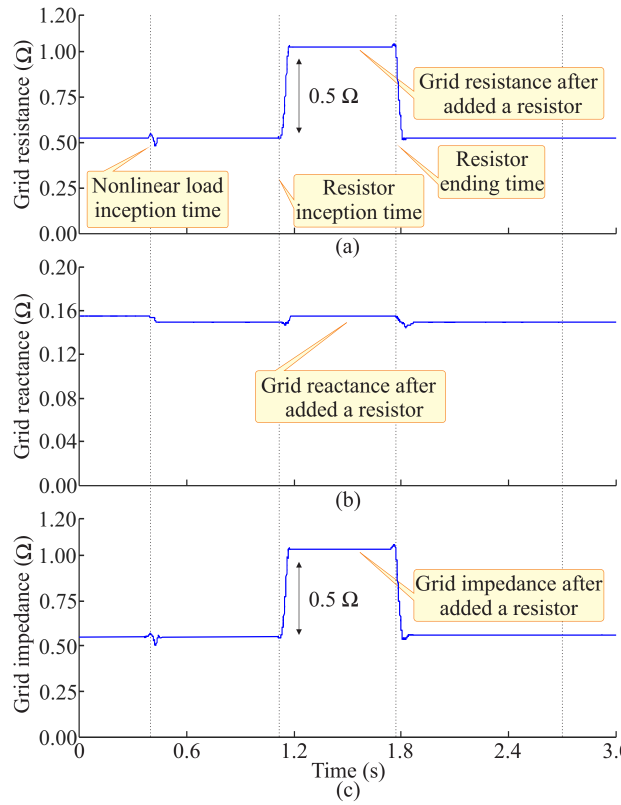

Fig. 4. Real-time grid impedance estimation with the interconnection of nonlinear load: (a) grid resistance; (b) grid reactance and; (c) grid impedance.

TABLE IV
SUMMARY OF THE EXPERIMENTAL RESULTS.

Scenarios	Phase	Step in grid impedance			Grid impedance	
		R (Ω)	X_L (Ω)	X_C (Ω)	R_g^w (Ω)	X_g^w (Ω)
I	-	↑0.50	↑0.188	-	1.20	0.37
	-	↓0.50	↓0.188	-	0.53	0.15
II	-	↑0.50	-	-	1.10	0.16
	-	↓0.50	-	-	0.53	0.16
III	A	↑0.50	↑0.188	-	1.25	0.37
		↓0.50	↓0.188	-	0.53	0.15
	B	↑0.50	↑0.188	-	1.10	0.36
		↓0.50	↓0.188	-	0.53	0.15
	C	-	-	-	0.52	0.16
		-	-	-	0.52	0.16
IV	-	↑0.50	↑0.188	-	1.10	0.38
	-	↑0.50	↑0.188	↑17.38	1.00	0.34

impedance estimation and DFT-based method were implemented, on the dSPACE 1103 PPC board, with a sampling rate of 1920 Hz to evaluate their computational burden. Table V summarizes both computational load in μs, per sampling. The proposed WBM, implemented through db(4) mother wavelet, presented a computational burden of 2.07μs, while the use of db(30) resulted in 4.32 μs. The grid impedance implemented via DFT method required 3.87 μs for providing only the grid impedance estimate. The recursive DFT-based method could also be implemented by using stored values of cosine and sine values in a buffer to minimize the computational burden, resulting in the execution time of 2.13 μs. Nevertheless, the proposed WBM implemented through db(4) presented the lowest computational burden.

TABLE V
COMPUTATIONAL BURDEN.

	DFT	db(4)	db(30)
Impedance estimation	3.87 μs 2.13* μs	2.07 μs -	4.32 μs -

*Recursive DFT.

This article has been accepted for publication in a future issue of this journal, but has not been fully edited. Content may change prior to final publication. Citation information: DOI 10.1109/TIE.2020.2972460, IEEE Transactions on Industrial Electronics

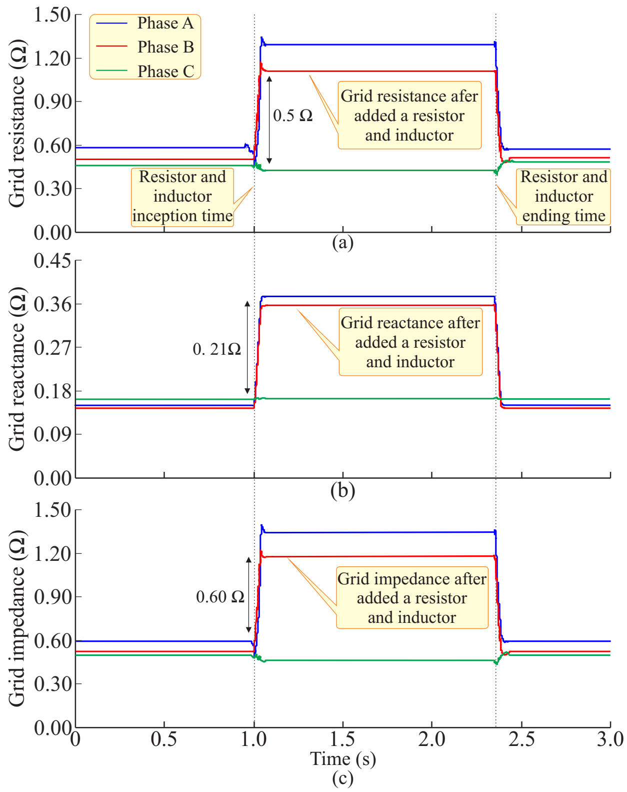

Fig. 5. Real-time grid impedance estimation with the unbalanced grid impedance: (a) grid resistance; (b) grid reactance and; (c) grid impedance.

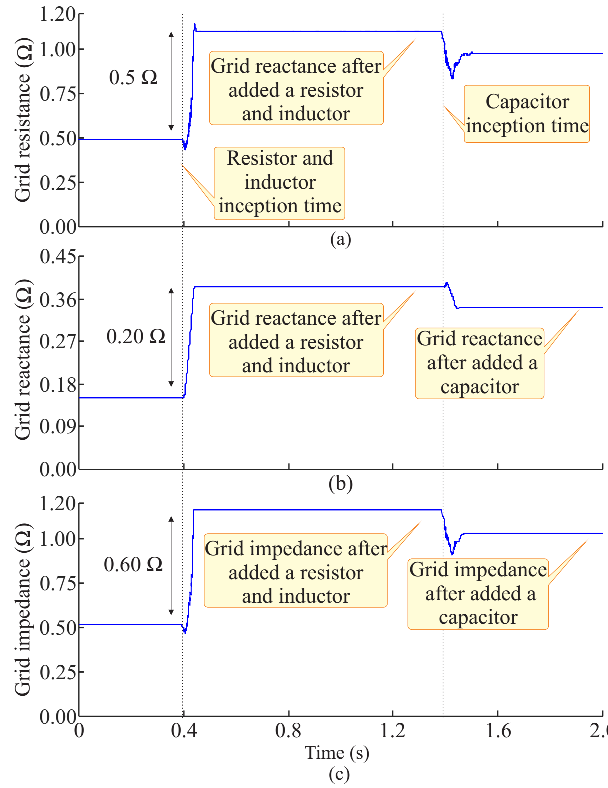

Fig. 6. Real-time grid impedance estimation with the interconnection of the capacitive load: (a) grid resistance; (b) grid reactance and; (c) grid impedance.

VII. Conclusion

This paper introduced a WBM for estimating the power grid-impedance, consisted of a WB-TDS and a WB-GIE, both implemented with RT-DWPT. When a grid changing occurs, the WB-TDS triggers the WB-GIE for injecting an interharmonic into the power grid to estimate the power grid impedance. This approach mitigates THD generated by the continuous signal injection employed in existing estimation techniques. This paper also presented the theoretical wavelet basis for implementing the WB-GIE, and the required adjusts for achieving accurate results. It also suggested a set of commissioning tests for determining the length of the mother wavelet, the interharmonic magnitude, and its duration. The experimental essays demonstrated that the proposed WBM provided an accurate grid impedance estimation of PCCs interconnected with standard loads, nonlinear loads, and capacitive banks. Besides, it is also effective under unbalanced operational conditions. Compared with existing methods, the proposed WBM provided reliable and fast grid transient detection and accurate grid impedance estimation. For its inherent characteristics, the proposed WBM should be further used in adaptive power flow control in distributed generation in low-voltage power systems.

References

[1] H. Liu, P. C. Loh, X. Wang, Y. Yang, W. Wang, and D. Xu, "Droop control with improved disturbance adaption for a pv system with two power conversion stages," *IEEE Trans. Ind. Electron.*, vol. 63, no. 10, pp. 6073–6085, Oct. 2016.

[2] G. Agundis-Tinajero, J. Segundo-Ramírez, N. Visairo-Cruz, M. Savaghebi, J. M. Guerrero, and E. Barocio, "Power flow modeling of islanded ac microgrids with hierarchical control," *Int. J. Electr. Power and Energy Syst.*, vol. 105, pp. 28–36, 2019.

[3] J. Rocabert, A. Luna, F. Blaabjerg, and P. Rodriguez, "Control of power converters in ac microgrids," *IEEE Trans. Power Electron.*, vol. 27, no. 11, pp. 4734–4749, Nov. 2012.

[4] J. C. Vasquez, J. M. Guerrero, A. Luna, P. Rodriguez, and R. Teodorescu, "Adaptive droop control applied to voltage-source inverters operating in grid-connected and islanded modes," *IEEE Trans. Ind. Electron.*, vol. 56, no. 10, pp. 4088–4096, Oct. 2009.

[5] M. Sumner, B. Palethorpe, D. W. P. Thomas, P. Zanchetta, and M. C. D. Piazza, "A technique for power supply harmonic impedance estimation using a controlled voltage disturbance," *IEEE Trans. Power Electron.*, vol. 17, no. 2, pp. 207–215, Mar. 2002.

[6] L. Asiminoaei, R. Teodorescu, F. Blaabjerg, and U. Borup, "Implementation and test of an online embedded grid impedance estimation technique for pv inverters," *IEEE Trans. Ind. Electron.*, vol. 52, no. 4, pp. 1136–1144, Aug. 2005.

[7] H. A. Pereira, F. D. Freijedo, M. M. Silva, V. F. Mendes, and R. Teodorescu, "Harmonic current prediction by impedance modeling of grid-tied inverters: A 1.4mw pv plant case study," *Int. J. Electr. Power and Energy Syst.*, vol. 93, pp. 30 – 38, 2017.

[8] M. Liserre, F. Blaabjerg, and R. Teodorescu, "Grid impedance estimation via excitation of lcl-filter resonance," *IEEE Trans. Ind. Appl.*, vol. 43, no. 5, pp. 1401–1407, Sept. 2007.

[9] S. Cobreces, E. J. Bueno, D. Pizarro, F. J. Rodriguez, and F. Huerta, "Grid impedance monitoring system for distributed power generation electronic interfaces," *IEEE Trans. Instrum. Meas.*, vol. 58, no. 9, pp. 3112–3121, Sept. 2009.

[10] N. Hoffmann and F. W. Fuchs, "Minimal invasive equivalent grid impedance estimation in inductive-resistive power networks using extended kalman filter," *IEEE Trans. Power Electron.*, vol. 29, no. 2, pp. 631–641, Feb. 2014.

[11] A. Ghanem, M. Rashed, M. Sumner, M. A. Elsayes, and I. I. I. Mansy, "Grid impedance estimation for islanding detection and adaptive control of converters," *IET Power Electron.*, vol. 10, no. 11, pp. 1279–1288,

Sept. 2017.

[12] M. Sumner, B. Palethorpe, and D. W. P. Thomas, "Impedance measurement for improved power quality-part 1: the measurement technique," *IEEE Trans. Power Del.*, vol. 19, no. 3, pp. 1442–1448, Jul. 2004.

[13] A. Vijayakumari, A. Devarajan, and N. Devarajan, "Decoupled control of grid connected inverter with dynamic online grid impedance measurements for micro grid applications," *Int. J. Electr. Power and Energy Syst.*, vol. 68, pp. 1 – 14, 2015.

[14] H. L. Monteiro, C. A. Duque, L. R. Silva, J. Meyer, R. Stiegler, A. Testa, and P. F. Ribeiro, "Harmonic impedance measurement based on short time current injections," *Elect. Power Syst. Res.*, vol. 148, pp. 108 – 116, 2017.

[15] M. Sumner, A. Abusorrah, D. Thomas, and P. Zanchetta, "Real time parameter estimation for power quality control and intelligent protection of grid-connected power electronic converters," *IEEE Trans. Smart Grid*, vol. 5, no. 4, pp. 1602–1607, Jul. 2014.

[16] F. C. A. Fernandes, R. L. C. van Spaendonck, and C. S. Burrus, "A new framework for complex wavelet transforms," *IEEE Trans. Signal Process.*, vol. 51, no. 7, pp. 1825–1837, Jul. 2003.

[17] D. K. Alves, R. Ribeiro, F. B. Costa, and T. O. A. Rocha, "Real-time wavelet-based grid impedance estimation method," *IEEE Trans. Ind. Electron.*, vol. 66, no. 10, pp. 8263–8265, Oct. 2019.

[18] M. A. Azzouz and E. F. El-Saadany, "Multivariable grid admittance identification for impedance stabilization of active distribution networks," *IEEE Trans. Smart Grid*, vol. 8, no. 3, pp. 1116–1128, May. 2017.

[19] P. García, M. Sumner, A. Navarro-Rodríguez, J. M. Guerrero, and J. Garcia, "Observer-based pulsed signal injection for grid impedance estimation in three-phase systems," *IEEE Trans. Ind. Electron.*, vol. 65, no. 10, pp. 7888–7899, Oct. 2018.

[20] C. B. Jacobina, M. B. R. Correa, R. F. Pinheiro, E. R. C. D. Silva, and A. M. N. Lima, "Modeling and control of unbalanced three-phase systems containing pwm converters," *IEEE Trans. Ind. Applicat.*, vol. 37, no. 6, pp. 1807–1816, Nov./Dec. 2001.

[21] F. B. Costa, "Boundary wavelet coefficients for real-time detection of transients induced by faults and power-quality disturbances," *IEEE Trans. Power Del.*, vol. 29, no. 6, pp. 2674–2687, Dec. 2014.

[22] "IEEE guide for planning dc links terminating at ac locations having low short-circuit capacities," *IEEE Std 1204-1997*, pp. 1–216, Jan. 1997.

[23] N. P. W. Strachan and D. Jovcic, "Stability of a variable-speed permanent magnet wind generator with weak ac grids," *IEEE Trans. Power Del.*, vol. 25, no. 4, pp. 2779–2788, Oct. 2010.

[24] D. K. Alves, F. B. Costa, R. L. A. Ribeiro, C. M. S. Neto, and T. O. A. Rocha, "Real-time power measurement using the maximal overlap discrete wavelet-packet transform," *IEEE Trans. Ind. Electron.*, vol. 64, no. 4, pp. 3177–3187, Apr. 2017.

[25] C. S. Burrus and A. G. G. H. Ramesh, *Introduction to Wavelets and Wavelet Transforms*. New Jersey, USA: Prentice Hall, 1998.

[26] *IEEE Standard Definitions for the Measurement of Electric Power Quantities Under Sinusoidal, Nonsinusoidal, Balanced, or Unbalanced Conditions*, Mar. 2010.

[27] R. P. Medeiros, F. B. Costa, and K. M. Silva, "Power transformer differential protection using the boundary discrete wavelet transform," *IEEE Trans. Power Del.*, vol. 31, no. 5, pp. 2083–2095, Oct. 2016.

Denis Keuton Alves was born in Frutuoso Gomes, Rio Grande do Norte, Brazil, in 1986. He received the B.Sc., M.Sc., and Ph.D. degrees in electrical engineering from the Federal University of Rio Grande do Norte, Brazil, in 2012, 2015, and 2019, respectively. He is currently a Substitute Teacher with the Federal Institute of Rio Grande do Norte, Santa Cruz, Brazil. His research interests include electric power quality, renewable energy systems, smart-grid solutions, as well as diagnosis and monitoring power quality.

Ricardo Lucio de Araujo Ribeiro (M'04-SM'19) was born in Campina Grande, Brazil, in 1961. He received the B.S., M.S., and Ph.D. degrees in electrical engineering from the Federal University of Campina Grande, Campina Grande, Brazil, in 1990, 1992, and 2003, respectively. From 2001 to 2002, he was with Department of Electrical Engineering, Politecnico di Torino, Turin, Italy, as a Visiting Scholar. Since March 2004, he has been with the Department of Electrical Engineering, the Federal University of Rio Grande do Norte, Natal, Brazil, as an Associate Professor and the Director of the Research Laboratory of Power Electronics and Renewable Energy-LEPER. His research interests include power electronics, renewable energy systems, power quality control, energy efficiency, ac/dc microgrids, storage systems, and power system stability. Dr. Ribeiro is Secretary of Joint Chapter - PES/IAS/PELS - IEEE Bahia Section R9, Tutor of the IEEE - IAS/PELS Student Branch of the Federal University of Rio Grande do Norte, Member of the IEEE Industrial Electronics and Power Electronics Society and SOBRAEP-Brazilian Association of Power Electronics.

Flavio Bezerra Costa (M'10) was born in Brazil, 1978. He earned his B.Sc., M.Sc., and Ph.D. degrees in Electrical Engineering from Federal University of Campina Grande (UFCG), Brazil, in 2005, 2006, and 2010, respectively. Currently, he is Professor at Federal University of Rio Grande do Norte (UFRN), Brazil. From 2010 to 2011, he was a postdoctoral fellow at UFCG. From December 2011 to March 2012, he was a visiting fellow at K. U. Leuven, Belgium. From June 2014 to July 2014, he was a visiting fellow at INESC Porto, Portugal. From August 2014 to September 2015, he was a postdoctoral fellow at the Rheinisch-Westfälische Technische Hochschule Aachen (RWTH AACHEN) University, Germany. From November 2018 to October 2019, he was visiting professor at TU Berlin, Germany. In the past 10 years, he has published more than 30 journal and 100 conference papers. His research interests lie in the broad area of generation, transmission and distribution systems, including power system protection, real-time analysis of power quality disturbances and faults, renewable energy systems, as well as smart-grid solutions.

Thiago de Oliveira Alves Rocha was born in Natal, Brazil, in 1986. He received the B.S., M.S., and Ph.D. degrees in electrical engineering from the Federal University of Rio Grande do Norte, Natal, Brazil, in 2011, 2013, and 2015, respectively. From October 2014 to June 2016, he was a Faculty Member with the Federal Institute of Rio Grande do Norte, João Câmara, Brazil. From June 2016 to July 2017, he has been with the Department of Electrical Engineering, Federal University of Pernambuco, Recife, Brazil, as an Adjunct Professor. Since July 2017, he has been with the Department of Electrical Engineering, Federal University of Rio Grande do Norte, Natal, Brazil, as an Adjunct Professor. Since June 2010, he has been a Researcher in the Laboratory of Industrial Electronics and Renewable Energy (LEIER/UFRN) and since July 2017 he has been the Adjunct Director of LEIER/UFRN. His research interests include renewable energy systems, power electronics, active power filters, and electrical drives. Dr. Rocha is a Member of the IEEE and SOBRAEP-Brazilian Association of Power Electronics.

Josep M. Guerrero (S'01-M'04-SM'08-FM'15) received the B.S. degree in telecommunications engineering, the M.S. degree in electronics engineering, and the Ph.D. degree in power electronics from the Technical University of Catalonia, Barcelona, in 1997, 2000 and 2003, respectively. Since 2011, he has been a Full Professor with the Department of Energy Technology, Aalborg University, Denmark, where he is responsible for the Microgrid Research Program (www.microgrids.et.aau.dk). From 2014 he is chair Professor in Shandong University; from 2015 he is a distinguished guest Professor in Hunan University; and from 2016 he is a visiting professor fellow at Aston University, UK, and a guest Professor at the Nanjing University of Posts and Telecommunications. From 2019, he became a Villum Investigator by The Villum Fonden, which supports the Center for Research on Microgrids (CROM) at Aalborg University, being Prof. Guerrero the founder and Director of the same centre.

His research interests is oriented to different microgrid aspects, including power electronics, distributed energy-storage systems, hierarchical and cooperative control, energy management systems, smart metering and the internet of things for AC/DC microgrid clusters and islanded minigrids. Specially focused on maritime microgrids for electrical ships, vessels, ferries and seaports. Prof. Guerrero is an Associate Editor for a number of IEEE TRANSACTIONS. He has published more than 500 journal papers in the fields of microgrids and renewable energy systems, which are cited more than 40,000 times. He received the best paper award of the IEEE Transactions on Energy Conversion for the period 2014-2015, and the best paper prize of IEEE-PES in 2015. As well, he received the best paper award of the Journal of Power Electronics in 2016. During six consecutive years, from 2014 to 2019, he was awarded by Clarivate Analytics (former Thomson Reuters) as Highly Cited Researcher. In 2015 he was elevated as IEEE Fellow for his contributions on "distributed power systems and microgrids."